Phys. Status Solidi B **252,** No. 7, 1486–1491 (2015) / **DOI** 10.1002/pssb.201552069

physica status solidi b
www.pss-b.com
basic solid state physics

Advances in the study of the deformation mechanism of stishovite

Keith M. Azzopardi[1], Jean-Pierre Brincat[1], Joseph N. Grima[2], and Ruben Gatt*[,1]

[1] Metamaterials Unit, Faculty of Science, University of Malta, Msida, MSD 2080, Malta
[2] Department of Chemistry, Faculty of Science, University of Malta, Msida, MSD 2080, Malta

Received 5 February 2015, revised 20 April 2015, accepted 22 April 2015
Published online 2 June 2015

Keywords auxetic behaviour, deformation mechanism, negative Poisson's ratios, stishovite

* Corresponding author: e-mail ruben.gatt@um.edu.mt, auxetic@um.edu.mt, Phone: +356 2340 2274

Stishovite, a mineral which is estimated to be abundant in the Earth's mantle, exhibits negative Poisson's ratios for a range of loading directions at specific ambient pressure ranges. Here, we investigate the deformation mechanisms which lead to auxetic behaviour in the (001) plane in further detail, and show that the two-dimensional projection of the structure is auxetic by the type α dilating rhombi mechanism. This corroborates the distorting octahedra three-dimensional mechanism described previously [Azzopardi et al., RSC Adv. **5**, 8974 (2015)].

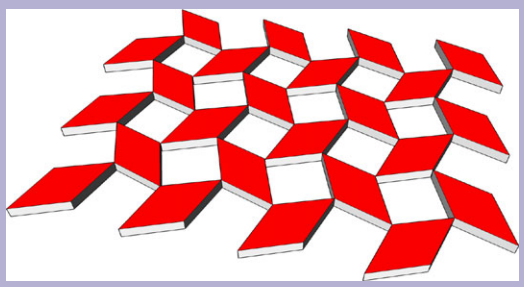

© 2015 WILEY-VCH Verlag GmbH & Co. KGaA, Weinheim

1 Introduction Seismology is a field in geophysics which deals with earthquakes, their predictions and the propagation of waves through the Earth. This critical field depends, however, on the accurate knowledge of the elastic moduli and the pressure dependence of the minerals which compose the mantle [1, 2]. One such mineral which is estimated to be a significant constituent of the Earth's mantle is stishovite [3–10].

Stishovite [11–16] is a rutile-type polymorph of silica, having the formula SiO_2. It has a hexa-coordinated tetragonal structure with a symmetry class of P42/mnm [17–22]. Stishovite is a rare mineral on the surface of the Earth, since it is only formed at pressures which are several hundred thousand times higher than atmospheric pressure. Such pressures can be encountered in meteorite impacts [23] and in the Earth's mantle. Due to the lack of its availability, stishovite has had an unusual history of being synthesised under laboratory conditions [24] before being discovered in nature [17], more than half a century ago.

Despite the relative lack of availability of the mineral, and the extremely high pressures involved, there have been a significant number of studies dedicated to stishovite. In fact, its structure at atmospheric pressure has been determined experimentally [25]. Furthermore, its mechanical properties, including its elastic constants, have also been determined at different pressures, both experimentally and through simulation [1, 2, 22, 26–29].

Recently, it has been shown that stishovite presents a negative Poisson's ratio for loading in specific directions in certain planes and at certain pressures [30]. This has far-reaching implications. Auxetic behaviour is not unknown in silica polymorphs [28, 31–33]. Another silicate polymorph called α-cristobalite is well known for exhibiting auxetic properties at atmospheric pressure [34, 35]. Stishovite can be produced directly from α-cristobalite by the application of pressure [9, 36].

Auxetic behaviour [37] is known to be the product of a particular geometry deforming by a specific deformation mechanism. Relevant examples of such mechanisms include the chiral mechanisms [38, 39], the dilation mechanism [40, 41], the rotating quadrilaterals mechanisms [42–46] and further modifications of these mechanisms such as the Type II rotating rectangles mechanism which has been used to describe auxeticity in α-cristobalite [47].

Auxeticity in the (001) plane of stishovite has been explained through a three-dimensional deformation

© 2015 WILEY-VCH Verlag GmbH & Co. KGaA, Weinheim

modelinvolving distortions of the constituent octahedra [30]. However, since the Poisson's ratio is a two-dimensional property, understanding the deformation mechanisms in two dimensions is essential when trying to design new materials which exhibit this property. In view of this, the work presented here investigates, through empirical simulations, the properties of the two two-dimensional systems which may be used to describe the projected structure of stishovite in the (001) plane; the wine-rack system (the projections of the Si–O bonds), and the fully open type α rotating rhombi system (the projections of the O–O interactions) [46]. The results obtained from these models will be compared to the real structure of stishovite [25] projected in the (001) plane.

2 Methodology

2.1 DFT calculations The structure of stishovite [25] was optimised at 0 GPa using DFT calculations. These simulations were conducted using the CASTEP [48] program in the Materials Studio package on a $1 \times 1 \times 1$ unit cell, and periodic boundary conditions were used throughout. To minimise symmetry constraints apart from those imposed by the unit cell itself, the space group was set to P1 rather than P42/mnm. Removing of the symmetry constrains resulted in a significant increase in the computational time of the simulations; however, this was mandatory for the current study as it was required that all elements of the cell act independently. Furthermore, geometry optimisations were conducted using the BFGS minimiser [49] as this allows for simultaneous relaxation of the internal degrees of freedom together with the cell parameters. Stringent convergence criteria were used as detailed in Azzopardi et al. [30]. These included an energy cut off of $5\,e^{-6}$ eV atom^{-1}, a maximum force of 0.01 eV Å^{-1}, a maximum stress of 0.02 GPa, and a maximum displacement of $5\,e^{-4}$ Å. The cut-off energy was found to be sufficient at 1000 eV. The Brillouin zone sampling was conducted by means of a Monkhorst-mesh grid [50] with a $4 \times 4 \times 6$ mesh. Norm conserving pseudopotentials were used for the simulations as included in the Materials Studio package.

The elastic constants were calculated by applying the constant-strain method, which involves applying a series of normal strains and shear strains, measuring the respective stress and using standard transformations to produce the stiffness matrix (the full set of elastic constants). The calculated elements of the stiffness matrix [*C*] were compared to those available in the published literature [1, 2, 22, 27, 28] and were found to coincide.

The angle of maximum auxeticity of stishovite in the (001) plane was found by calculating and plotting the off-axis Poisson's ratio. Additional simulations were performed by stressing the structure in the (001) plane along the direction of minimum Poisson's ratio. In each additional simulation, the structure was subjected to a series of geometry optimisations when being stressed by up to 0.2% of the Young's modulus in the direction of minimum Poisson's ratio. Detailed measurements of bond lengths, bond angles and inter-atom distances were obtained to study the deformation mechanisms.

2.2 EMUDA simulations The EMUDA methodology has been used in the past to study the auxeticity of structures constructed from dummy atoms. The method followed here is based on the work of Grima et al. [51] The two-dimensional structure of stishovite projected in the (001) plane was constructed in the Materials Studio package. The resulting structure may be described as an open wine-rack structure, with the Si atoms being the nodes of the structure.

If the O–Si–O angles are kept rigid while the Si–O bonds are allowed to change their length, the structure will deform by dilation. On the other hand, if the bond lengths are fixed while the bond angles are allowed to change, the structure will deform by hinging.

If the interactions of the Si–O bonds and the O–Si–O angles are not considered, the projection of the octahedra results in a pair of rhombi with oxygen atoms at their vertices, and O–O interactions forming their edges. These rhombi may be described as the type α connected rhombi [46]. Referring to Fig. 1, the O atoms 1, 2, 3 and 4 form rhombus 'A', while atoms 4, 5, 6 and 7 form rhombus 'B'. The major axis of rhombus 'A' (1–3 in Fig. 1) is parallel to the secondary axis of rhombus 'B' (5–7 in Fig. 1), and *vice versa*.

Simulations were conducted using the Forcite module. Six dummy atoms per unit cell and four force–field types were used. The two different silicon atoms in one unit cell were labelled as force-field type 'A' or 'C', while types 'B' or 'D' were each assigned once to two oxygen atoms in the unit cell.

The projections of the silica octahedra in the (001) plane were also represented by including bonds between the different

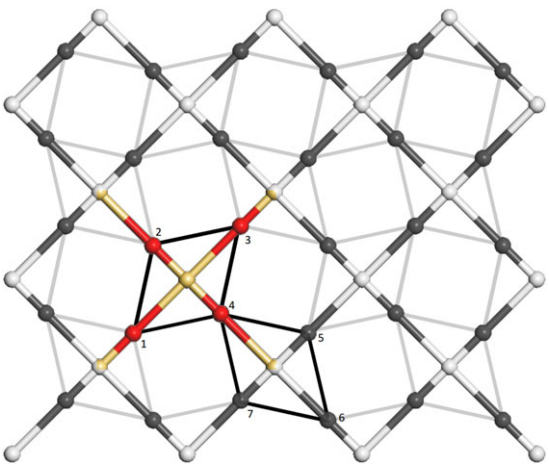

Figure 1 Projection into the (001) plane of all the atoms in the structure of stishovite. The red and black atoms represent oxygen, while the yellow and light grey atoms represent silicon. The black lines, which are meant to guide the eye, show the 'rotating rhombi' model, and represent the octahedra in three-dimensional structure.

© 2015 WILEY-VCH Verlag GmbH & Co. KGaA, Weinheim

oxygen atoms (numbered atoms in Fig. 1). The O–O distances and O–O–O angles were calculated through restraints. The deformation mechanism of the structure was controlled by altering the rigidity and stiffness of the bond angles and bond lengths inside the structure, as detailed in Table 1. The Si–O–Si angles were fixed at 180° in all simulations.

A first set of simulations was performed by keeping the O–Si–O angles rigid, and the Si–O bonds soft. In these cases, no stiffness was given to the O–O bonds and O–O–O angles, thus having a system which may be described as a dilating wine-rack. Subsequent simulations were performed where the rigidity of the O–Si–O angles and the stiffness of the Si–O bonds were changed simultaneously. Details are given in Table 1.

A second set of simulations was then performed by keeping the O–O–O angles rigid and the O–O bonds soft. In these cases, no stiffness was given to the Si–O bonds and O–Si–O angles, thus creating a system which may be described as a dilating type α connected rhombi system. Also in this case, subsequent simulations were performed where the rigidity of the O–O–O angles and the stiffness of the O–O bonds were changed simultaneously as shown in Table 1.

3 Results

3.1 Comparison of DFT simulations with experimental results The structure of stishovite obtained through DFT calculations was compared to the experimentally derived coordinates presented by Ross [25]. The fractional coordinates were found to coincide to a very high degree of precision.

The calculated off-axis Poisson's ratios were also compared to the experimental values. These calculated parameters were also found to have no significant differences when compared to the experimental values, as shown in Fig. 2.

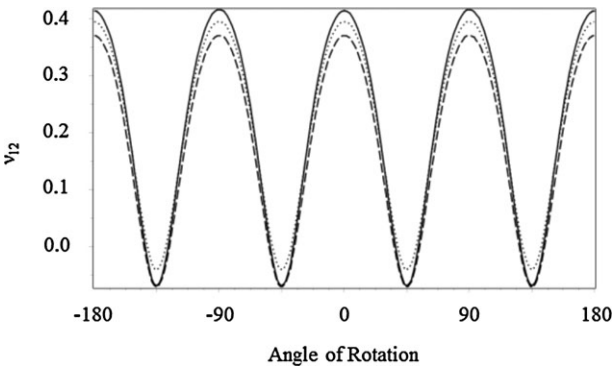

Figure 2 Variation of the Poisson's ratio in the (001) plane of stishovite with loading direction. The solid line represents the experimental data obtained by Weidner et al. [2], the dashed line represents the experimental data obtained by Brazhkin et al. [27], while the dotted line represents the results obtained in the current work.

3.2 The wine-rack model When considering the EMUDA simulations performed without the inter-atomic distances constrained (i.e. the wine-rack structure), three deformation mechanisms are possible: dilation of the bonds, hinging of the bond angles, and a combination of both dilation and hinging. Simulation number 1, as listed in Table 1, allowed the two-dimensional structure to deform solely through dilation of the bonds. Simulation number 5 allowed the structure to deform solely through hinging of the bonds angles. Simulations 2 through 4 allowed both modes simultaneously at various degrees of rigidity or stiffness. The results of these simulations are given in Fig. 3a and b.

Figure 3a shows the variation in the Poisson's ratio with changing loading direction for a wine-rack structure deforming through dilation of the bonds. When the pure dilational model is considered, a Poisson's ratio of -1 is observed for loading on-axis, while a ratio of 0 is observed for loading off-axis. The wine-rack structure deforming by dilation is therefore auxetic when loading on-axis. When loading in this direction, a component of the applied force is present in all the Si–O bonds, and hence all the Si–O bonds elongate, leading to the observed auxetic behaviour. A Poisson's ratio of 0 is observed for loading at 45° off-axis since at this angle all the

Table 1 The complete set of EMUDA simulations performed. Note that angle stiffness has units of kcal mol^{-1} rad^{-2} while bond rigidity has units of kcal mol^{-1} Å^{-2}.

simulation No.	Si–O bond stiffness	O–O bond stiffness	O–Si–O angle rigidity	O–O–O angle rigidity
1	10	OFF	999	OFF
2	10	OFF	50	OFF
3	10	OFF	10	OFF
4	50	OFF	10	OFF
5	999	OFF	10	OFF
6	OFF	10	OFF	999
7	OFF	10	OFF	50
8	OFF	10	OFF	10
9	OFF	50	OFF	10
10	OFF	999	OFF	10

© 2015 WILEY-VCH Verlag GmbH & Co. KGaA, Weinheim

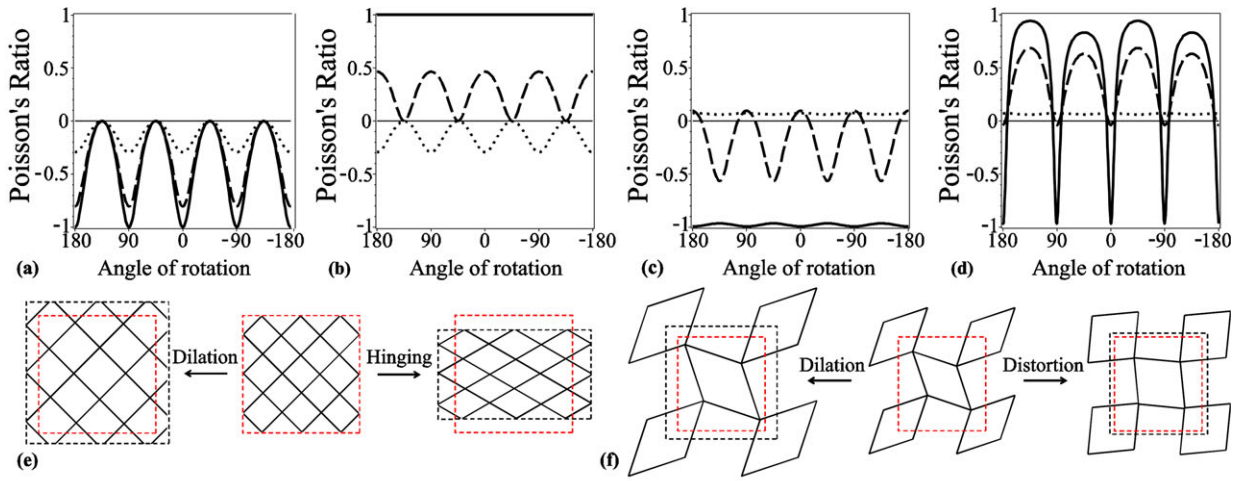

Figure 3 Calculated variation of the Poisson's ratio of the EMUDA model with loading direction, when considering the deformation mode attributable to (a) the wine-rack structure deforming by pure dilation [solid line: simulation 1; dashed line: simulation 2; dotted line: simulation 3], (b) the wine-rack structure deforming by pure hinging [solid line: simulation 5; dashed line: simulation 4; dotted line: simulation 3], (c) the rhombi structure deforming by pure dilation [solid line: simulation 6; dashed line: simulation 7; dotted line: simulation 8], (d) the rhombi structure deforming by pure distortion [solid line: simulation 10; dashed line: simulation 9; dotted line: simulation 8]. (e) Visualisation of the idealised dilation and hinging models for the wine-rack structure when a tensile load is applied in a horizontal direction, (f) visualisation of the idealised dilation and distortion models for the rhombi structure when a tensile load is applied in a horizontal direction.

force applied remains in the Si–O bonds parallel to the loading direction. No component of the applied force is translated to the Si–O bonds which are orthogonal to the loading direction, and hence they do not elongate.

Figure 3b shows the variation in the Poisson's ratio with changing loading direction for a wine-rack structure deforming through hinging. When the structure is constrained to deform solely through hinging, a constant Poisson's ratio of 1 is observed across all possible loading directions. This is an effect of the constraints present in the structure and the rules of geometry.

When the two mechanisms discussed previously are allowed to act concurrently, a system with intermediate mechanical properties is obtained. As is shown by the dotted lines in Fig. 3a and b, when the two mechanisms are of equal importance, the Poisson's ratio fluctuates between -0.25 *circa* for loading on-axis, and 0 for loading off-axis.

3.3 The fully open type α connected rhombi model The results of the EMUDA simulations performed with the inter-atomic distances constraints in place (i.e. the rhombi model) are discussed next. In the case of the type α connected rhombi model, three different deformation mechanisms are again possible: dilation of the rhombi, distortion of the rhombi (a change solely in the angles within the rhombi) and a combination of both mechanisms acting concurrently. Rotations of the rhombi are not possible since the structure is already in its most open form, and is hence locked to rotations.

In simulation 6, the rhombi-constrained structure was allowed to deform solely through dilation of the rhombi, in simulation 10 only distortion of the rhombi was allowed, while both modes simultaneously at various degrees of stiffness or rigidity were allowed in simulations 7 through 9. The results of these simulations are given in Fig. 3c and d.

Figure 3c shows the Poisson's ratios observed when the structure in Fig. 1 is allowed to deform though dilation of the rhombi. When this dilation is the sole mechanism acting, a Poisson's ratio of *circa* -1 is obtained for all loading directions. This expected observation can be understood in light of the fact that the internal angles of the rhombi are constrained at specific values, which implies that if one side of either rhombus lengthens, then the other sides must lengthen to the same degree.

Figure 3d shows the Poisson's ratios obtained when the distortion deformation mechanism is allowed. This is the most interesting of the four plots. When the structure is loaded on-axis, the structure presents a Poisson's ratio close to -1. This, however, rises sharply to very positive values as the loading direction is moved off-axis. The reason for this is that when the structure is loaded on-axis, the applied force causes both rhombi to contract along their primary axis, as their angles start to approach right angles. Since the rhombi are arranged alternately, a contraction is observed in two different directions (see Fig. 3f). This causes the observed negative Poisson's ratio. When the plane is loaded off-axis, the rhombus which has its major axis aligned along the loading direction elongates: its major axis becomes longer while its secondary axis becomes shorter since there is no component of the applied force across it. At the same time the second rhombus shortens along its main axis and elongates along its secondary axis. Since the two primary

© 2015 WILEY-VCH Verlag GmbH & Co. KGaA, Weinheim

axes of the two rhombi are alternate, this causes an amplification of the effect, and results in the observed rapid change to a positive Poisson's ratio.

Furthermore, it is also interesting to note that both the dilation and distortion mechanisms produce a negative Poisson's ratio for loading on-axis when acting individually. However, when these two deformation mechanisms are allowed to act concurrently, a positive Poisson's ratio is produced for loading off-axis, as shown by the dotted line in Fig. 3c and d.

3.4 Application to stishovite Two approaches can be employed to determine which of the two-dimensional deformation mechanisms are actually occurring when stishovite deforms. The first approach involves measuring inter-atomic distances in the DFT model and analysing these in detail. The second approach involves comparing the experimental and DFT-calculated off-axis Poisson's ratios to those obtained using EMUDA modelling.

Starting with the first of these two approaches, a number of distances and angles were obtained from the DFT simulations of the three-dimensional structure of stishovite projected onto the (001) plane. The first set of measurements made was that of the O–Si–O angles at all the investigated levels of applied stress. These O–Si–O angles did not change at all, which is a clear indication that the structure does not deform through wine-rack hinging.

The second set of measurements obtained were those of the Si–O bond lengths. The Si–O bonds aligned along the direction of applied stress increase or decrease in length as stress is applied in tension and in compression respectively. The Si–O bonds perpendicular to the direction of applied stress do not change in length. This set of observations precludes deformation by wine-rack hinging as a deformation mechanism of importance.

The third set of measurements obtained were the O–O inter-atomic distances. These data are plotted in Fig. 4a. All four O–O inter-atomic distances in the same rhombus increased exactly to the same extent. Hence, only one point per rhombus is given in Fig. 4a. However, the O–O distances in the rhombus which has its main axis aligned closer to the direction of applied stress (rhombus 4567) increased more significantly than those of rhombus 1234. This seems to indicate that deformation by rhombi dilation might be happening to some extent.

The final set of measurements obtained were the internal O–O–O inter-atomic angles. These internal O–O–O angles were observed to change, as plotted in Fig. 4b. As expected, the internal O–O–O angles in the rhombus which has its main axis aligned close to the direction of applied stress (rhombus 4567) change more than those of rhombus 1234. This seems to indicate that deformation by rhombi distortion might be happening to some extent.

When these sets of measurements are taken together, it is evident that the projected structure of stishovite does not deform through wine-rack hinging or deformation, but rather through concurrent dilation and distortion of the fully open type α rotating rhombi.

This conclusion is confirmed when utilizing the second approach for determining which of the two-dimensional deformation mechanisms are actually occurring when stishovite deforms. It was observed that the Poisson's ratio obtained for loading of the stishovite structure in the (001) plane (Fig. 2) is only negative for loading off-axis, with positive ratios being obtained when loading on-axis. In the EMUDA modelling carried out, this pattern was only obtained in the off-axis plots of the rhombi model deforming through dilation and distortion concurrently. This confirms that these two mechanisms may be responsible for the deformation of stishovite when it is loaded in the (001) plane.

The conclusions reached should also be understood in light of the three-dimensional structure of stishovite. The projected rhombi represent the silicate octahedra present in stishovite. Azzopardi et al. [30] had concluded that the auxetic behaviour present in this plane can be attributed to a 'scissoring distortion' of the octahedra. When projected

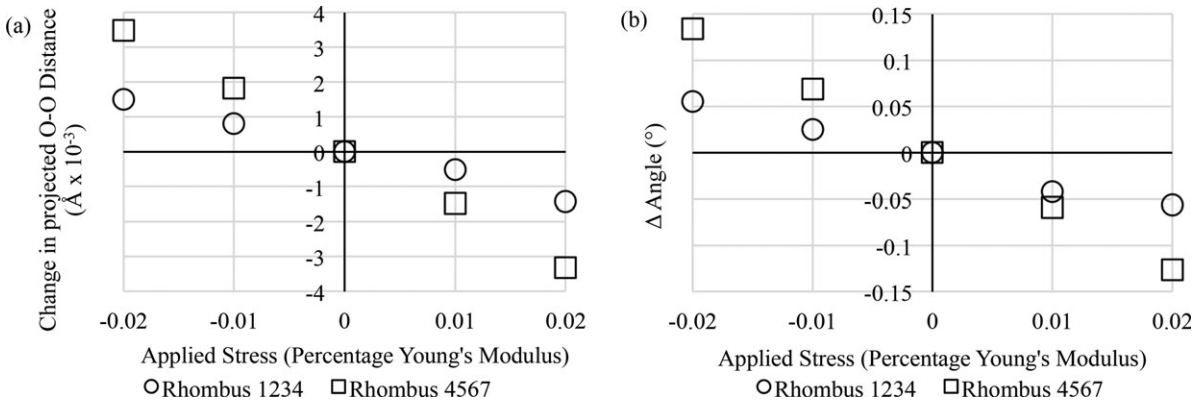

Figure 4 (a) Variation of the change in the projected O–O distances with the applied stress, calculated as a percentage of the Young's modulus. (b) Variation of the change in the projected O–O–O angles with the applied stress, calculated as a percentage of the Young's modulus. 'rhombus 1234' and 'rhombus 4567' are shown in Fig. 1.

© 2015 WILEY-VCH Verlag GmbH & Co. KGaA, Weinheim

onto a plane, this scissoring distortion would appear as a dilation and distortion of the resulting rhombi. This work therefore corroborates the results presented in the previous work, and *vice versa*, with the important addition of having now described the same deformation mechanism in simpler, two-dimensional terms.

4 Conclusion The work presented here has shown that the deformation of the projected structure of stishovite into the (001) plane can be explained through concurrent dilation and distortion of the fully open type α rotating rhombi model. Both the projected structure created through DFT modelling and validated against the experimental structure, and the empirical model based on an idealised structure produced similar profiles for the Poisson's ratio.

The distortion of the idealised model can result in auxetic behaviour for loading in certain directions. This can be considered as a new way for this geometry to give rise to auxetic behaviour.

Acknowledgements This research has been carried out using computational facilities procured through the European Regional Development Fund, Project ERDF-080 'A Supercomputing Laboratory for the University of Malta'.

References

[1] B. B. Karki, L. Stixrude, and J. Crain, Geophys. Res. Lett. **24**, 3269 (1997).
[2] D. J. Weidner, J. D. Bass, A. E. Ringwood, and W. Sinclair, J. Geophys. Res. **87**, 4740 (1982).
[3] W. A. Bassett and J. D. Barnett, Phys. Earth Planet. Int. **3**, 54 (1970).
[4] R. C. Liebermann, A. E. Ringwood, and A. Major, Earth Planet. Sci. Lett. **32**, 127 (1976).
[5] T. Yagi and S.-I. Akimoto, Tectonophysics **35**, 259 (1976).
[6] C. Lee and X. Gonze, Phys. Rev. Lett. **72**, 1686 (1994).
[7] B. Li, S. M. Rigden, and R. C. Liebermann, Phys. Earth Planet. Int. **96**, 113 (1996).
[8] E. A. Goresy, L. Dubrovinsky, T. G. Sharp, S. K. Saxena, and M. Chen, Science **288**, 1632 (2000).
[9] L. Huang, M. Durandurdu, and J. Kieffer, Nature Mater. **5**, 977 (2006).
[10] A. Verma and B. Karki, Phys. Rev. B **79**, 214115 (2009).
[11] M. A. Carpenter, R. J. Hemley, and H. Mao, J. Geophys. Res. **105**, 10807 (2000).
[12] K. J. Kingma, R. E. Cohen, R. J. Hemley, and H. Mao, Nature **374**, 243 (1995).
[13] C. Lee and X. Gonze, J. Phys.: Condens. Matter **7**, 3693 (1995).
[14] D. Andrault, G. Fiquet, F. Guyot, and M. Hanfland, Science **282**, 720 (1998).
[15] D. M. Teter, R. J. Hemley, G. Kresse, and J. Hafner, Phys. Rev. Lett. **80**, 2145 (1998).
[16] V. V. Brazhkin, L. E. McNeil, M. Grimsditch, N. A. Bendeliani, T. I. Dyuzheva, and L. M. Lityagina, J. Phys.: Condens. Matter **17**, 1869 (2005).
[17] E. C. T. Chao, J. J. Fahey, J. Littler, and D. J. Milton, Geophys. Res. **67**, 419 (1962).
[18] W. Sinclair and A. E. Ringwood, Nature **272**, 714 (1978).
[19] F. Liu, H. Garofalini, D. King-Smith, and D. Vanderbilt, Phys. Rev. B **49**, 12528 (1994).
[20] S. R. Shieh, T. S. Duffy, and B. Li, Phys. Rev. Lett. **89**, 255507 (2002).
[21] T. Yamanaka, T. Fukuda, and J. Tsuchida, Phys. Chem. Miner. **29**, 633 (2002).
[22] F. Jiang, G. D. Gwanmesia, T. I. Dyuzheva, and T. S. Duffy, Phys. Earth Planet. Int. **172**, 235 (2009).
[23] I. P. Baziotis, Y. Liu, P. S. DeCarli, H. J. Melosh, H. Y. McSween, R. J. Bodnar, and L. A. Taylor, Nature Commun. **4**, 1404 (2013).
[24] S. M. Stishov and S. V. Popova, Geokhimiya **10**, 837 (1961).
[25] N. L. Ross, J. F. Shu, R. M. Hazen, and T. Gasparik, Am. Mineral. **75**, 739 (1990).
[26] A. K. Singh, D. Andrault, and P. Bouvier, Phys. Earth Planet. Int. **208–209**, 1 (2012).
[27] V. V. Brazhkin, M. Grimsditch, I. Guedes, N. A. Bendeliani, T. I. Dyuzheva, and L. M. Lityagina, Phys.–Usp. **45**, 447 (2002).
[28] B. Holm and R. Ahuja, J. Chem. Phys. **111**, 2071 (1999).
[29] A. Bosak, I. Fischer, M. Krisch, V. Brazhkin, T. Dyuzheva, B. Winkler, D. Wilson, D. Weidner, K. Refson, and V. Milman, Geophys. Res. Lett. **36**, L19309 (2009).
[30] K. M. Azzopardi, J. P. Brincat, J. N. Grima, and R. Gatt, RSC Adv. **5**, 8974 (2015).
[31] J. N. Grima, R. Jackson, A. Alderson, and K. E. Evans, Adv. Mater. **12**, 1912 (2000).
[32] J. N. Grima, R. Gatt, N. Ravirala, A. Alderson, and K. E. Evans, Mater. Sci. Eng. A **423**, 214 (2006).
[33] F. Scarpa, S. Blain, T. Lew, D. Perrott, M. Ruzzene and J. R. Yates, Composites A **38**, 280 (2007).
[34] A. Yeganeh-Haeri, D. J. Weidner, and J. B. Parise, Science **257**, 650 (1992).
[35] J. N. Grima, A. Alderson, and K. E. Evans, J. Phys. Soc. Jpn. **74**, 1341 (2005).
[36] D. D. Klug, R. Rousseau, K. Uehara, M. Bernasconi, Y. Le Page, and J. Tse, Phys. Rev. B **63**, 104106 (2001).
[37] R. S. Lakes, Science **235**, 1038 (1987).
[38] K. W. Wojciechowski, Mol. Phys. **61**, 1247 (1987).
[39] O. Sigmund, S. Torquato, and I. A. Aksay, J. Mater. Res. **13**, 1038 (1998).
[40] K. W. Wojciechowski, J. Phys. A **36**, 11765 (2003).
[41] A. Alderson and K. E. Evans, Phys. Chem. Miner. **28**, 711 (2001).
[42] J. N. Grima and K. E. Evans, J. Mater. Sci. Lett. **19**, 1563 (2000).
[43] J. N. Grima, R. Gatt, A. Alderson, and K. E. Evans, J. Phys. Soc. Jpn. **74**, 2866 (2005).
[44] J. N. Grima, A. Alderson, and K. E. Evans, Phys. Status Solidi B **242**, 561 (2005).
[45] J. N. Grima and K. E. Evans, J. Mater. Sci. **41**, 3193 (2006).
[46] J. N. Grima, P. S. Farrugia, R. Gatt, and D. Attard, Phys. Status Solidi B **245**, 521 (2008).
[47] J. N. Grima, R. Gatt, A. Alderson, and K. E. Evans, Mater. Sci. Eng. A **423**, 219 (2005).
[48] S. J. Clark, M. D. Segall, C. J. Pickard, P. J. Hasnip, M. I. J. Probert, K. Refson, and M. C. Payne, Z. Kristallogr. **220**, 567 (2005).
[49] B. G. Pfrommer, M. Cote, S. G. Louie, and M. L. Cohen, J. Comput. Phys. **131**, 233 (1997).
[50] H. J. Monkhorst and J. D. Pack, Phys. Rev. B **13**, 5188 (1976); Phys. Rev. B **16**, 1748 (1977).
[51] J. N. Grima, R. Gatt, T. G. C. Bray, A. Alderson, and K. E. Evans, Mol. Simulat. **31**, 915 (2005).

© 2015 WILEY-VCH Verlag GmbH & Co. KGaA, Weinheim